ELSEVIER

Journal of Neuroscience Methods 170 (2008) 35–44

JOURNAL OF NEUROSCIENCE METHODS

www.elsevier.com/locate/jneumeth

Hardware and methodology for targeting single brain arterioles for photothrombotic stroke on an upright microscope

Albrecht Sigler [a,b], Alexander Goroshkov [c], Timothy H. Murphy [a,b,d,*]

[a] *Kinsmen Laboratory of Neurological Research, Department of Psychiatry, 2255 Wesbrook Mall, University of British Columbia, Vancouver, BC, V6T 1Z3 Canada*

[b] *Brain Research Center, 2211 Wesbrook Mall, University of British Columbia, Vancouver, BC, V6T 2B5 Canada*

[c] *In vivo Imaging Centre, Life Sciences Institute, 2350 Health Sciences Mall, University of British Columbia, Vancouver, BC, V6T 1Z3 Canada*

[d] *Department of Cellular and Physiological Sciences, 2255 Wesbrook Mall, University of British Columbia, Vancouver, BC, V6T 1Z3 Canada*

Received 9 October 2007; received in revised form 18 December 2007; accepted 21 December 2007

Abstract

Investigators have begun to probe the role of individual surface arterioles in maintaining both the structure and function of cortical regions using vessel-specific clotting by *in vivo* photothrombosis after craniotomy in mice. To induce targeted strokes we describe a simple adaptation of a commercial upright Olympus BX51WI microscope, permitting light from a 532 nm laser to be directed into the back aperture of a high numerical aperture fluorescence objective. The system involves using a filter slot available on an Olympus BX series microscope to direct a collimated laser beam through the normal epifluorescence path to the objective back aperture resulting in focused photoactivation, with lateral and axial dimensions less than 3 and 5 μm, respectively. Existing fluorescence filters and dichroic mirrors are employed permitting one to safely target the green laser beam and view the clotting process based as red epifluorescence, either through the eye pieces or using a CCD camera. Interruption in blood flow can be confirmed using laser speckle microscopy. The positioning of the photothrombotic laser in this manner does not impede subsequent analysis of brain microcirculation using two-photon microscopy or other imaging methods. It is conceivable that this modification and laser system can also be used for other scenarios where targeted photoactivation or photobleaching would be required.

Keywords: Two-photon imaging: Stroke; *In vivo*; Photothrombosis; Dendrite; Neurovascular unit; Speckle imaging; Mouse; Imaging; Ischemia; Intrinisic signal imaging

1. Introduction

Photothrombosis provides a method of inducing targeted ischemia based on light-induced production of reactive oxygen species and triggering of clotting cascades (Watson et al., 1985). Importantly, the photothrombotic method can be performed with simple intraperitoneal or intravenous injection of a photosensitizer such as Rose Bengal followed by excitation of the dye with green light. To induce a targeted stroke, one merely needs to selectively illuminate the brain to activate the photosensitizer. Kleinfeld and colleagues (Schaffer et al., 2006) have used a targeted 532 nm laser directed through the two-photon microscope's excitation path to photoactivate individual surface arterioles (Kleinfeld et al., 2008). Such a method as adapted by us permitted the induction of local stroke and examination of relationships between cortical structure, function, and blood flow (Zhang and Murphy, 2007). The method is relatively precise since targeting a single arteriole can lead to a deficit that can only affects a subset of a cortical functional domain such as the forelimb (Zhang and Murphy, 2007), or in the case of penetrating arterioles, a region of only about 0.4 mm^2 of cortical surface (Nishimura et al., 2007). The approach has advantages over traditional wide-field photothrombosis since only small segments of arterioles are photoactivated (<10 μm), reducing the possibility of complications such as photoactivator-induced extravasation and inflammation. Here we describe a simple hardware device for a commercial microscope that enables targeted photothrombosis of individual surface arterioles through an existing red epifluorescence filter set. This method has the benefit of being relatively inexpensive

* Corresponding author at: Department of Psychiatry, 4N1-2255 Wesbrook Mall, University of British Columbia, Vancouver, BC, V6T 1Z3 Canada. Tel.: +1 604 822 0705; fax: +1 604 822 7981.

E-mail address: thmurphy@interchange.ubc.ca (T.H. Murphy).

0165-0270/$ – see front matter © 2008 Elsevier B.V. All rights reserved.
doi:10.1016/j.jneumeth.2007.12.015

to implement and permits direct and continuous examination of the light-induced clotting process using epifluorescence. Examination of the clotting process allows one to verify its efficacy and specificity. It is anticipated that this hardware modification could be extended to ultraviolet lasers and used to photoactivate a variety of agents including photoactivatable GFPs (Ando et al., 2004). Another use is as a bleaching device allowing changes in donor fluorescence to be quantified during Förster resonance energy transfer (Biskup et al., 2004), or uncaging compounds such as tetracyclines to locally induce protein expression (Cambridge et al., 2006), using lasers of appropriate wavelength.

2. Methods

2.1. Animal model

Adult, urethane-anesthetized mice aged 2–5 months and weighing 24–32 g were used for all experiments. Animal protocols were approved by the University of British Columbia Animal Care Committee and were consistent with Canadian Council for Animal Care guidelines. Briefly, anesthesia was induced with urethane (0.12%, w/w) and body temperature was maintained at $37 \pm 0.5\,^{\circ}C$ using a heating pad and feedback regulation from a rectal temperature probe. A craniotomy was performed over the right somatosensory cortex while custom-made ear and tooth bars held the anesthetized mouse. The skull was fastened to a stainless steel plate (Kleinfeld and Denk, 2000) with cyanoacrylate glue and dental cement, which was then attached to 25.4 mm rods that were mounted on an aluminum plate that could be moved on and off the Olympus BX51WI microscope. In order to minimize movement artifact (due to breathing and heart rate), the exposed brain was covered with 1–1.5% agarose (Type 3-A Sigma; A9793) dissolved in a HEPES buffered (pH 7.3) physiological salt solution (in mM): 135 NaCl, 5.4 KCl, 1 $MgCl_2$, 1.8 $CaCl_2$, and 5 HEPES, and sealed with a custom cut glass coverslip. Furthermore, consistent with the targeted nature of Rose Bengal-induced strokes we have not found that brain regions which control cardiovascular function are affected during local stroke (no noticeable change in heart rate or respiration during targeted strokes). Assessment of blood oxygen saturation (on average >90%), heart rate (400–600 beats/min), and breathing rate (~200 breaths/min) in a subset of animals indicated that under the conditions we used for imaging, physiological parameters were relatively constant over the course of our experiments. All animals were under urethane anesthesia and breathing air as described by us and others (Kleinfeld and Denk, 2005; Zhang and Murphy, 2007). The physiological parameters mentioned above were measured using a Mouse-Ox pulse oximeter (Starr Life Sciences, Oakmont, PA). Hydration was maintained by intraperitoneal injection of saline (100–200 μl) with 20 mM glucose at 1–2 h intervals.

2.2. Stroke model

For the Rose Bengal photothrombosis model (Watson et al., 1985), we injected the dye (0.03 mg/g mouse body weight, diluted to 10 mg/ml in HEPES buffered artificial CSF) into the tail vein using a 28 1/2-gauge needle after warming the tail with a lamp. If intravenous injection should be not possible, 0.1 mg/g mouse dye also could be injected intraperitoneally. Nonetheless, we prefer tail vein injection since blood concentration of dye is elevated immediately preventing the need to perform prolonged photoactivation that may increase non-specific effects. If some off-target photoactivation should be observed even after intravenous injection, we suggest investigators reduce the intravenous Rose Bengal concentration to 0.01 mg/g mouse. Photoactivation then has to be performed promptly because the Rose Bengal clears after intravenous injection with a τ of less than 3 min (Zhang and Murphy, 2007). To target individual surface arterioles we used a 0.7–1.4 mW (measured at the objective back aperture) 532 nm beam from a diode pumped laser (Beta Electronics MGM-20, Columbus, OH) that was coupled to the microscope's epifluorescence light path and focused into a spot through a 40×, 0.8 NA water immersion lens as described in detail in this paper (Fig. 1) and in (Zhang and Murphy, 2007). For laser illumination individual arterioles supplying the forelimb or hindlimb areas were identified from their appearance and response during intrinsic optical signal (IOS) imaging (Frostig et al., 1990) and were targeted at multiple points to reduce redundant paths of surface blood flow (Schaffer et al., 2006). In practice, it is favorable to rotate between targeted sites after 1–2 min to ensure that clots are initiated at each site by a relatively high concentration of dye since it clears rapidly.

2.3. Laser speckle imaging

To periodically assess blood flow, we performed laser speckle imaging as previously described (Briers and Webster, 1996; Dunn et al., 2001) using a Dalsa M60 Pantera camera (Dalsa, Waterloo, ON) mounted on the upright microscope used for photoactivation. Laser speckle imaging of blood flow is based on blurring of interference patterns of scattered laser light, by flowing blood (Briers and Webster, 1996; Dunn et al., 2001). For illumination, a 784 nm 32 mW StockerYale SNF-XXX-785S-35 laser (Stocker & Yale, Salem, NH) with an Edmund anamorphic beam expander T47274 (Edmund Optics, Barrington, NJ) was held directly on a micromanipulator at an angle of 30° and directed at the brain surface that was enclosed by a coverslip and agarose and viewed with a 4×0.075 NA objective. Typically, we collected 100–300 images at 10 Hz using 10 ms exposure. Individual images of variance were created in ImageJ (National Institute of Mental Health, Bethesda, MD) using its two-dimensional variance filter (3×3 or 5×5 pixel kernel size, 3.47 μm/pixel). Following variance filtering all images were averaged, and a single 32-bit-image of the standard deviation was produced by taking the square root of the averaged variance image. The standard deviation image was then divided by the mean of all the raw images to help correct for uneven illumination and to create an image of speckle contrast (standard deviation/mean). Alternatively, blood flow can be imaged with two-photon microscopy of fluorescent dextran in the blood

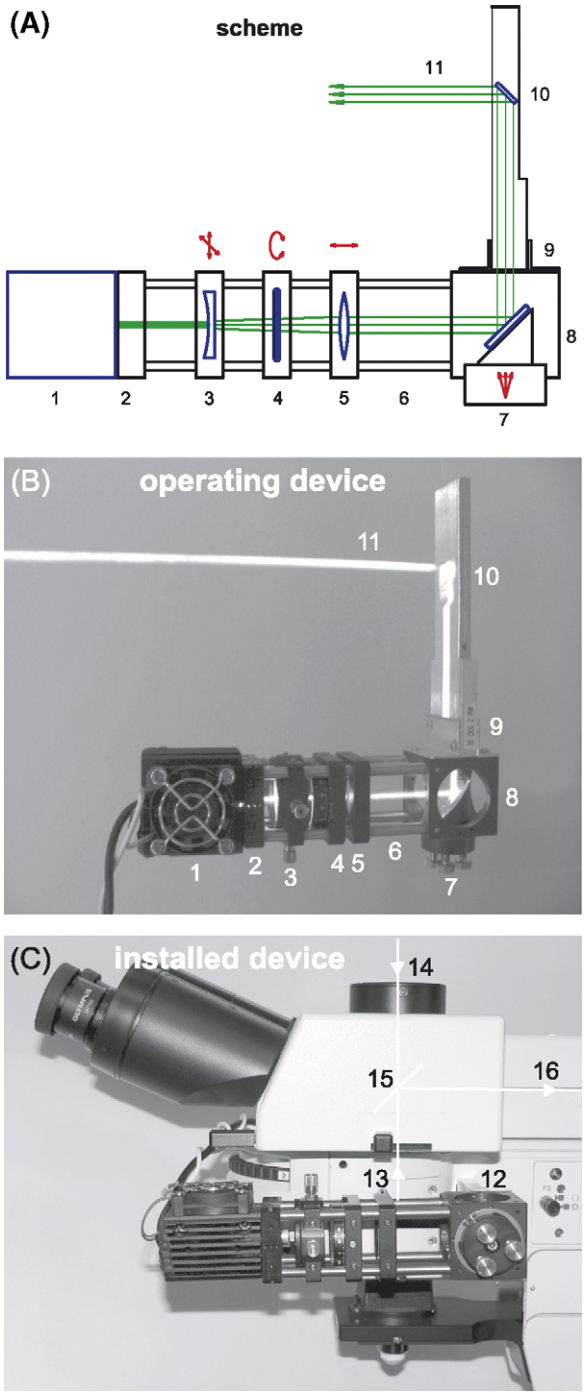

Fig. 1. Modification of an upright microscope for photoactivation. (A) Schematic drawing of a photoactivation/bleaching device compatible with an Olympus microscope and designed to insert into an existing filter slot within the epifluorescence pathway. The components of the device are: (1) the laser; (2) fixing plate for the laser; (3) concave lens to widen the laser beam (placed 26 mm from laser output); (4) polarizer to attenuate the light; (5) convex lens to collimate the beam (67 mm from laser output); (6) cage assembly rods; (7) beam steering mirror with adjustable position to target the light focus; (8) cube to hold the adjustable mirror device; (9) aluminum angles to connect the mirror bearing cube to the slider insert; (10) slider to insert the device into the filter slot of a microscope with a 9 mm fixed mirror that reflects (11) the laser beam path into the epifluorescence train of the microscope. (B) Photograph showing the device and its components labeled as in panel A. The path of the laser beam (11) has been made visible by scattering of its light with fog. Note: the device should not be turned on in this manner without careful eye protection since the beam is directly accessible and potentially dangerous (Ajudua and Mello, 2007). We show it in this way to illustrate the beam path only and emphasize that for safe operation the system should be enclosed. (C) The laser bleaching/photoactivation device is shown inserted into an existing filter slot of an Olympus BX51WI microscope. The emitted light of the laser (fan on top) is directed into the microscope's epifluorescence path (12) with the device drawn in panel A, shown separately in panel B. Hidden, inside the microscope are: (13) the epifluorescence filter cube; (14) the path of two-photon excitation light; (15) the DPMC-WI mirror; (16) the light path to the CCD camera. Part numbers correspond to the ones in the part list (Table 1).

plasma (Kleinfeld and Denk, 2000; Kleinfeld et al., 1998; Zhang et al., 2005).

2.4. Lateral and axial resolution of photoactivation

To estimate the lateral dimension of the photoactivated area, we bleached spots in an orange fluorescent plastic slide (Chroma Technology, Rockingham, VT, USA) with the 532 nm laser and then subsequently determined the size of these spots with two-photon microscopy using an Olympus IR-LUMPlanFl water-immersion objective (40×/0.8 NA) that we also use for photoactivation. For two-photon microscopy we used a Coherent Mira 900 laser (Coherent, Santa Clara, CA, USA) pumped by a 5-W Verdi laser and tuned to 900 nm to excite the sample. Images were acquired by custom software (IgorPro; Wavemetrics, Portland, OR, USA). To determine the axial dimension of the focal volume in which the photoactivation process occurs (and to confirm its lateral size that we also estimated using bleaching techniques), we imaged the fluorescence of a Texas Red dextran labeled agarose slab (~0.5 mg/ml dye in 2% agarose gel) while moving the objective with 1 μm steps in the axial direction. The laser spot size in the *Z*-direction then was estimated by taking the derivative of the plot of fluorescence signal versus scanning depth.

3. Results

3.1. Construction of a compact laser photoactivation system

To perform photothrombosis within single arterioles in initial experiments we found that green excitation light (532 nm) on the order of 1–3 mW was required (Schaffer et al., 2006; Zhang and Murphy, 2007). Therefore, to ensure adequate photothrombosis given losses of light through coupling optics, we have chosen to base our system on a 20 mW diode pumped solid state 532 nm laser MGM-20 (Beta Electronics, Columbus, OH). The laser system includes a fan and heat sink as well as a TTL triggered power supply. The first step in construction was tapping the heat sink of the laser to accept 8–32 bolts (Fig. 1A and B, part 1). We then attached a Thorlabs 30 mm square microbench SP02 system plate (Thorlabs, Newton, NJ) to the base of the laser heat sink as shown in Fig. 1A and B, part 2. Four 100 mm Thorlabs rods with 6 mm diameter were then inserted into the 30 mm plate base. Onto the rods we attached a series of beam conditioning optics using 30 mm microbench parts. A Galilean

Table 1
List of the parts for modification of an Olympus BX51WI microscope for laser-induced photoactivation

1	532 nm diode pumped solid-state laser (Beta Electronics, MGM-20)
2	Threaded cage plate (Thorlabs, SP02)
3	30 mm cage *XY*-translator for 1-in. optics (Thorlabs, HPT1) with Plano-concave lens, 25.4 mm diameter, A-coated, focal length 30 mm (Thorlabs, LC2679-A)
4	30 mm cage compatible rotation mount (Thorlabs, CRM1) with Linear polarizing glass filter, diameter 25.4 mm (Edmund Optics, NT54-926)
5	Threaded cage plate (Thorlabs, SP02) with Plano-convex lens, 25.4 mm diameter, A-coated, focal length 75.0 mm (Edmund Optics LA1608-A)
6	6 mm cage assembly rods, length 102 mm, 4 pieces (Thorlabs, ER3)
7	Beam steering mirror holder, 30 mm (Linos, G065087000) with visible laser diode mirror, 20 mm diameter (Edmund Optics, NT46-619)
8	Microbench cube, 30 mm (Linos, G061081000)
9	Aluminum angles, equal leg 12.7 mm × 12.7 mm, length 40 mm, 2 pieces (Metalsupermarkets, 6063-T52)
10	Aluminum insert (custom made as shown in Fig. 2) with First surface silver mirror, square, 9 mm × 9 mm, 1 mm thickness (Edmund Optics, NT31-004)

telescope, which consists of a positive and a negative lens, was used both to expand the beam and to provide the opportunity to correct for beam divergence at the distance of the objective back aperture. The first lens in the Galilean telescope (closest to laser; Fig. 1A and B, part 3) was a −30 mm concave lens placed just after the laser aperture (26 mm from it), and the second one (Fig. 1A and B, part 5) was a 75 mm positive convex lens 67 mm from the laser aperture. The distance between the conditioning lenses was adjusted to achieve a collimated laser beam at the location of the objective back aperture when the device was inserted into the microscope. To attenuate the laser power, a polarizer (Edmund Optics) was included within the beam path on a Thorlabs microbench CRM1 rotating mount (Fig. 1A and B, part 4). Rotation of the polarizer reduced the light power by up to 93%. To provide for additional adjustment of beam position, the first microbench lens mount included *XY* offset using the Thorlabs microbench HPT1 lens holder (Fig. 1A and B, part 5). To angle the laser into the microscope and to provide an additional degree of adjustment we added a Linos 30 mm cube (Linos Photonics, Göttingen, Germany; Fig. 1A and B part 8) on the end of four 100 mm rods (Fig. 1A and B, parts 6–7), which contained a solid silver (coated) mirror with angle adjustment (Fig. 1A and B, part 7). To direct the beam into the microscope's epifluorescence excitation path (the path the arc lamp takes), we used an existing 7.3 mm filter slot in the Olympus BX51WI upright microscope (Fig. 1C). To guide the laser, a piece of aluminum, 140 mm long, 41.2 mm wide, 9.52 mm thick, was machined as in Fig. 2 to fit within the filter slot. A slot was cut into the aluminum stock to provide a path for the beam, and a 45-degree angle was cut in which to glue (i.e. with cyanoacrylate glue) a square 9 mm × 9 mm, 1 mm thick solid silver mirror (Fig. 1A and B, part 10) to direct the laser toward the objective back aperture (Fig. 2). The aluminum light guide was attached with custom 1.6 mm aluminum angles (Metalsupermarkets, Mississauga, Ont., Canada; Fig. 1A and B, part 9) with M3 screws to the Linos 30 mm cube (Fig. 1A and B, part 8). Using this arrangement, the laser follows a U-shaped path where it makes two 90-degree turns to end up parallel to the fluorescence excitation path. Importantly, the device can be easily removed from the microscope and returned back within seconds to make the beam path available for fluorescence excitation with a conventional arc lamp if required. For a list of parts, see Table 1.

3.2. Beam characteristics

After constructing the laser, we installed it into the microscope and tuned the beam position and diameter using a combination of the movable lenses and solid mirror placed in the 30 mm Thorlabs tube. The diameter of the beam was adjusted as needed by moving the −30 and 75 mm lenses. To simplify the adjustment process, we fixed the position of one lens and adjusted the second lens only. We chose the Galilean telescope concave/convex lens system to reduce the length of the optical path and thus to create a more compact device reducing torsional strain.

The beam diameter at the exit point of the device (directed toward the microscope fluorescence excitation path) was estimated on a millimeter scale using a commercial photo camera to be 2.8 mm and is less than 3 μm after being focused by a high NA objective (see Fig. 3 for images of the laser spot on a vessel and Fig. 6 for *in situ* calibration using test specimens). It should be noted that larger or smaller beam diameters can be obtained by adjusting the ratio of focal lengths of the two conditioning lenses. The −30 mm and 75 mm lens combination

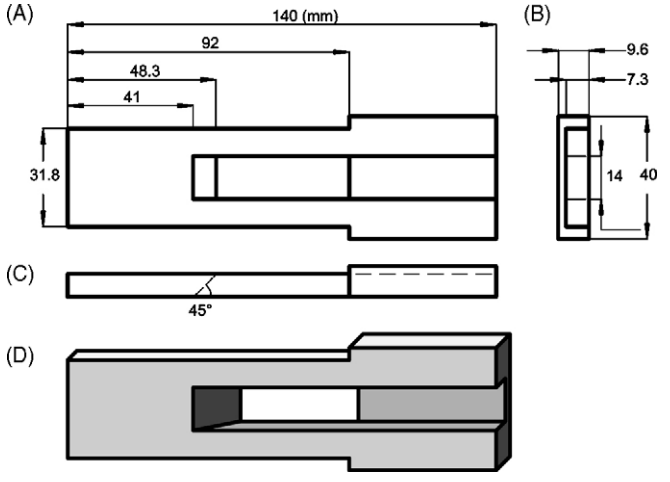

Fig. 2. Layout of the laser insert for an Olympus microscope (BX51WI). (A) Drawing of the device as it would be viewed when inserted into the microscope from the user's perspective. (B) Drawing of the end view. (C) Drawing of the view from top edge. (D) 3D view. Suggested material: aluminum, all measures are in mm. A CAD drawing of this insert is available upon request.

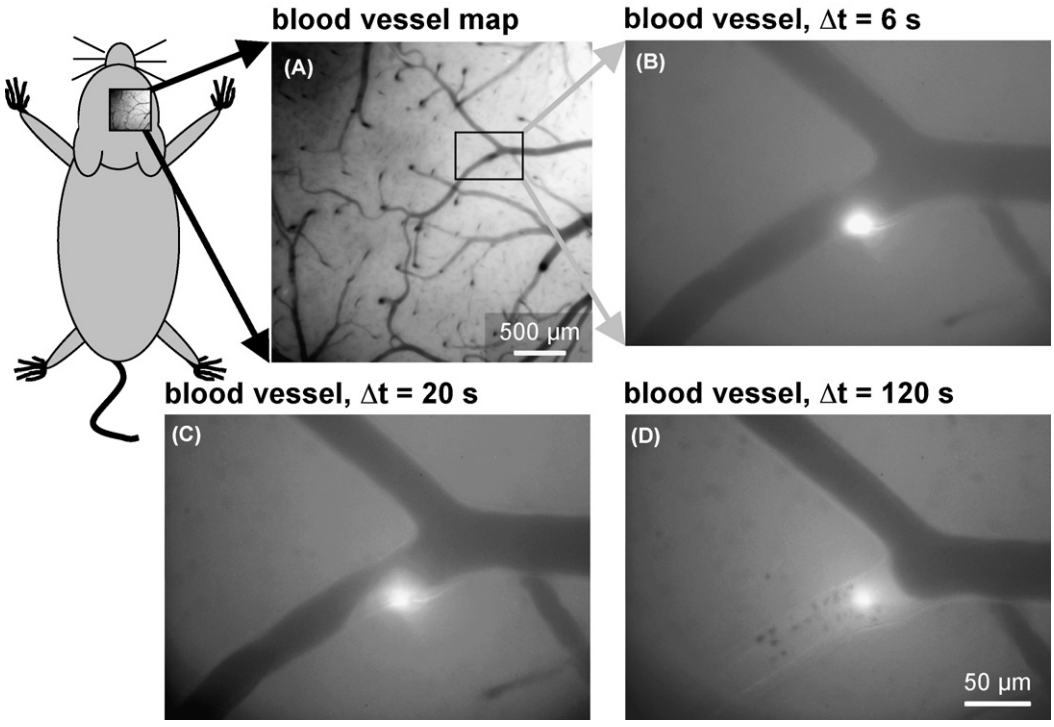

Fig. 3. Targeting individual brain arterioles for photoactivation of Rose Bengal. (A) Schematic showing experimental subject (C57 Bl6 mouse) and brain vasculature with regions for photoactivation indicated by arrows. (B) Photoactivation spot visualized by Rose Bengal fluorescence following excitation with 532 nm laser light in the arteriole segment shown in panel A. The arterioles are made visible as dark structures due to dim illumination with blue background light (cut-off wavelength 480 nm). The original 12-bit image was scaled nonlinear to visualize both the very dim background structure as well as the laser spot, which showed several orders of magnitude higher intensity. To produce a background level of light sufficient to view vasculature for presentation purposes, we used a blue excitation filter with cut-off wavelengths 395 and 480 nm (Edmund Optics, #NT46-541). This filter when combined with the Olympus rhodamine filter set U-MWG2 allows for some violet colored light to be detected by the CCD camera permitting vessels to be visible by adjustment of image brightness and contrast. The dim violet colored light should not photoactivate Rose Bengal within the specimen. However, we did not use background illumination for any actual experiments; we used it only for recording of presentation images to make blood vessels visible. (C and D) Subsequent images of the specimen shown in B during further fluorescence activation by laser light. The blood flow in the arteriole at the left bottom of the image was blocked within 2 min of photoactivation with green laser light. See also Supplemental Movie.

we have used should increase beam diameter by approximately 2.5-fold. After reflection by the fixed mirror (Fig. 1A and B, part 10), the laser beam does not pass through any additional lens in the microscope before entering the objective back aperture. If, in other microscope types, there is an additional lens, possible beam divergence could be compensated by adjusting the distance between the two lenses of the laser device (with the device inserted into the microscope) until the laser is collimated at the objective back aperture. Beam dimensions were adjusted interactively by moving lens position slightly. The beam diameter at the position of the objective back aperture after all microscope optics, but before the objective was 3.5 mm. Beam collimation was confirmed by projecting the beam through all microscope optics (except the objective) to a distance of about 3 m. For adjusting the beam properties we used high attenuation with the polarizer to increase laser safety. The MGM-20 532 nm laser can also be gated using a TTL pulse providing another means of attenuating laser power and controlling it in an automated manner. To ensure proper laser safety all adjustments of power were performed using 532 nm laser safe glasses and a power meter. Lastly, to improve laser safety the entire device can be encased within 1 mm thick black anodized aluminum.

3.3. Setting up targeting

Once the desired beam size and power have been obtained (using measurements made near the objective back aperture), one can begin to consider photoactivation of individual arterioles (Fig. 3). Before working with an animal, we have found it useful to examine standard epifluorescence test specimens. For test slides we typically employ a red fluorescent plastic slide (Chroma Technology, Rockingham, VT). To prevent saturation of detectors, such as the CCD camera, or to provide better viewing by eye, we typically attenuate the laser maximally since extremely strong epifluorescence was observed with test slides. Using the test slide, we could determine where within the microscope field the photoactivation spot would fall. The spot could then be moved to a small degree using the positioning mirror within the 30 mm cube or the adjustment of lens position (Fig. 1A and B, part 5 or 7). The range of adjustment here is not high, given the requirement of positioning the beam on the fixed mirror within the aluminum stock that inserts within the microscope's slot (Fig. 1A and B, part 10). We have found it useful to mark the photoactivation spot on a CCD camera display using a piece of adhesive tape. For CCD camera imaging on the same system that employs two-photon microscopy, we use the

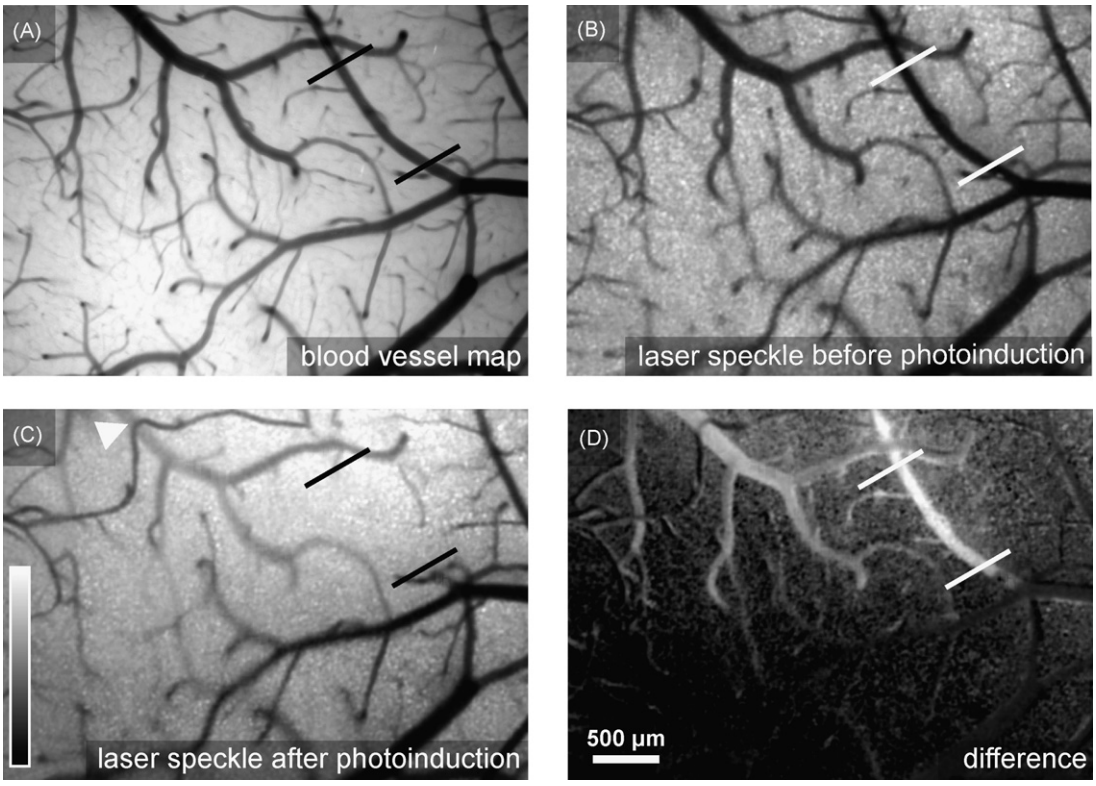

Fig. 4. Using laser speckle imaging to track photoactivation of Rose Bengal within individual brain arterioles. (A) Map of mouse surface vasculature, taken under green light to increase vessel contrast in light reflection (taken before Rose Bengal injection). The arteriole segments where photoactivation will be performed are indicated by two lines. (B) Laser speckle standard deviation image with dark tones indicating higher velocities of blood flow. Again, the vessel to be targeted by the 532 nm laser is indicated by two lines. (C) Laser speckle variance image after photoactivation within the indicated arterial segment. The targeted arteriole (position indicated) is now not visible, indicating that flow through it has become negligible. Interestingly, an adjacent venule indicated by a white arrow on the left of the flow-blocked arteriole also shows increased speckle variance; perhaps reflecting reduced drainage from areas supplied by the targeted arteriole. The calibration bar indicates the ratio of speckle standard deviation to the mean reflectance in a range of 0.02–0.08. (D) Speckle difference image; laser speckle post photoactivation (C) minus pre-photoactivation (B), with white areas showing vessels exhibiting slowed blood flow. The difference image indicates that the greatest degree of flow change occurs in the targeted arteriole and its nearby venules.

Olympus WI-DPMC dual port camera adapter. This adapter has three positions: (1) a clear aperture that permits unobstructed two-photon microscopy; (2) a path with 100% of light transmission to a CCD camera; (3) a position for use of the eyepieces. To effectively use the WI-DPMC adapter, two modifications were made: (1) the IR reflecting mirror to direct light to the rear camera was replaced by a solid silver mirror; (2) a neutral density filter placed on the 0.5× camera relay lens was removed. The neutral density filter was apparently placed by Olympus to balance brightness observed on a CCD camera display when switching between 0.5× and 4× relay lenses. In this case the 0.5× relay lens was attenuated (by the neutral density filter) to match the image brightness of the 4× relay. To get more signal we removed the neutral density filter. For photoactivation we found that standard Texas Red or rhodamine filter sets were generally usable. However, in some cases, commercial red epifluorescence filter sets do not permit good transmission of 532 nm laser light. In this case, investigators may need to remove their excitation filter or replace it with one that permits transmission of 532 nm light. The emission spectrum of Rose Bengal is broad (Du et al., 1998) and thus can be monitored easily with most red epifluorescence filter sets.

3.4. Blocking a vessel in vivo

After aligning the laser and determining the approximate position (within the microscope field) of the photoactivation spot using a fluorescent test slide (i.e. Chroma plastic slide), we were then ready to proceed with an animal experiment (Fig. 3A–D). Using an anesthetized mouse with a craniotomy preparation, we first performed baseline measurements of blood flow using laser speckle microscopy (Fig. 4). Given that the photoactivatable Rose Bengal will be injected, we use a blue filter within our dissecting scope light source to view the specimen to avoid spurious photoactivation with green or white light. We also avoid two-photon imaging just after injecting Rose Bengal (typically within the first 10 min) since it can be weakly excited and potentially spuriously photoactivated using 900 nm light employed for two-photon imaging of GFP (Zhang and Murphy, 2007). Regional laser speckle imaging of blood flow was performed as previously described by us and others (Dunn et al., 2001; Zhang and Murphy, 2007). By examining laser speckle images and images of blood vessels taken previously (before Rose Bengal injection) under illumination with green LEDs (Main Electronics, Vancouver, BC, Canada; #KFB 1340), we then selected

individual arterioles based on their position, size, and shape (Fig. 4A). The green LEDs were mounted using an aluminum collar around the 4× objective. The peak wavelength of the LED was 525 nm, which provides enhanced contrast between blood and brain. Arterioles were identified that were presumably branches of the middle cerebral artery. They were distinct from venules based on their size and branching patterns. Using a motorized stage with the ability to store various *X*, *Y*, and *Z* positions we then targeted at least two or three sites along the arteriole for photothrombosis. In previous studies we have found it necessary to target multiple sites along the arteriole for photothrombosis (Zhang and Murphy, 2007) since there is potential for collateral or even reversing flow that can prevent a single occlusion site from having a significant effect on the local blood supply (Schaffer et al., 2006). The laser was then focused on the vessel and then turned on. Individual arterioles were illuminated for typically 1 min each. To facilitate blocking, arterioles were photoactivated several times. Clot formation was facilitated by focusing the laser on the vessel wall and not on its lumen (see Supplemental material/Movie 1). Focusing the laser on the vessel wall helped to nucleate the clotting process. Because Rose Bengal is rapidly ($\tau = 175$ s) cleared from the blood (Zhang and Murphy, 2007), we typically performed all photoactivation within 10 min of intravenous injection of a 5 mg/ml solution of Rose Bengal. Clotting was easily confirmed by direct visual examination or using a CCD camera. For safe viewing of the clotting process, the CCD camera and trinocular microscope tube are positioned behind the dichroic mirror and the emission filter on the fluorescence filter cube. Since the laser employed is of solid-state construction, we could merely switch it on and off to control the photoactivation process. As mentioned earlier, the process could be further modulated using the laser's TTL gating function. We should emphasize that individual investigators need to be certain that no significant green laser light can leak through to the eye pieces before viewing the photoactivation process with unprotected eyes since the laser beam could case severe retina damage (Ajudua and Mello, 2007).

3.5. Laser speckle imaging to confirm occlusion

We used laser speckle imaging (Briers and Webster, 1996; Dunn et al., 2001) to monitor blood flow in the vessels targeted for photothrombotic occlusion. To perform laser speckle imaging, we used direct illumination by an external infrared laser (784 nm) to generate a speckle pattern due to scattering of coherent laser light by the brain. This laser is mounted directly on the microscope stage and does not employ any microscope optics and thus should not interfere with the optical path for photothrombosis or other forms of imaging. Blood flow blurs the speckle pattern since objects that produce the scattering are constantly moving. We quantified the blurring by determining the local standard deviation for each pixel over a 3×3 or 5×5 pixel neighborhood, as in (Briers and Webster, 1996; Dunn et al., 2001). Prior to Rose Bengal photoactivation, the laser speckle image shows regions with higher blood flow velocity as darker gray tones, which indicate a lower local standard deviation (Fig. 4B). We then used this method to assess blood flow changes in targeted vessels (Fig. 4D). Arterioles blocked by photothrombosis became invisible with the laser speckle imaging, indicating a very low flow velocity (Fig. 4C). To better resolve the blood flow changes, we calculated images showing the difference between speckle images recorded before and after photoactivation. This approach also indicated a reduction of venous blood flow to the left of the targeted arteriole area (Fig. 4D). Thus, laser speckle imaging can be used to confirm the photothrombotic blockade of blood flow with the device we describe here and in (Zhang and Murphy, 2007).

3.6. Resolution of the photoactivation process and avoidance of spurious photoactivation

In targeting surface arterioles one concern is spurious off-target photoactivation of both adjacent and deeper vessels. Fortunately the arterioles, which feed the subsurface cortex, run along the pial surface allowing them to be selectively targeted relative to deeper arterioles or nearby surface venules. To estimate in lateral direction the size of the photoactivation spot, we used the 532 nm laser to bleach a fluorescent plastic slide (Fig. 5A). Two-photon analysis of the bleached slide indicated a lateral resolution of 2.8 μm, measured as average half width of the bleached spot in the *X* and *Y* dimensions (Fig. 5C). We have also examined the excitation spot size resulting from using a homogeneous specimen such as a slab of Texas Red dextran labeled 2% agarose gel (Fig. 5B). For fluorescent agarose the average of *X* and *Y* resolution was 2.9 μm (measured at half maximal intensity; Fig. 5D). Since targeted vessels were generally greater than 20 μm in diameter, lateral spread of light should be minimal.

A second concern is photoactivation of vessels beneath the vessel that is targeted. To address this point, we estimated the Z-resolution of the photoactivation laser by examining the relationship between the focus position and the intensity of the homogeneously fluorescent slab of Texas Red dextran labeled agarose gel. We estimated that the laser Z-resolution was 4.4 μm by determining the half-width of the derivative of the relationship between focal position and intensity (Fig. 5E). Again, given that targeted vessels were greater than 20 μm in diameter, we would not expect significant penetration of light below the vessel that was targeted. To further address this point, we also determined whether the targeted vessels themselves would absorb a significant amount of the green photoactivation light, thus screening underlying tissue and vasculature from out of focus photoactivation. To perform this analysis we focused the green photoactivation laser on a surface arteriole and examined scattered light in neighboring tissues flanking the arteriole (Fig. 6A and B). A 30% reflecting and 70% transmitting mirror was used to examine scattered laser light reflected by the surface of the brain. This analysis revealed that when the photoactivation laser was focused on an arteriole, light scattering at the focal spot was reduced by an average of $54 \pm 17\%$, compared to focusing the light on the adjacent brain that lacked major vessels (Fig. 6). Examination of intensity profile shoulder regions (that made a transition between the targeted vessel and the tissue) indicated

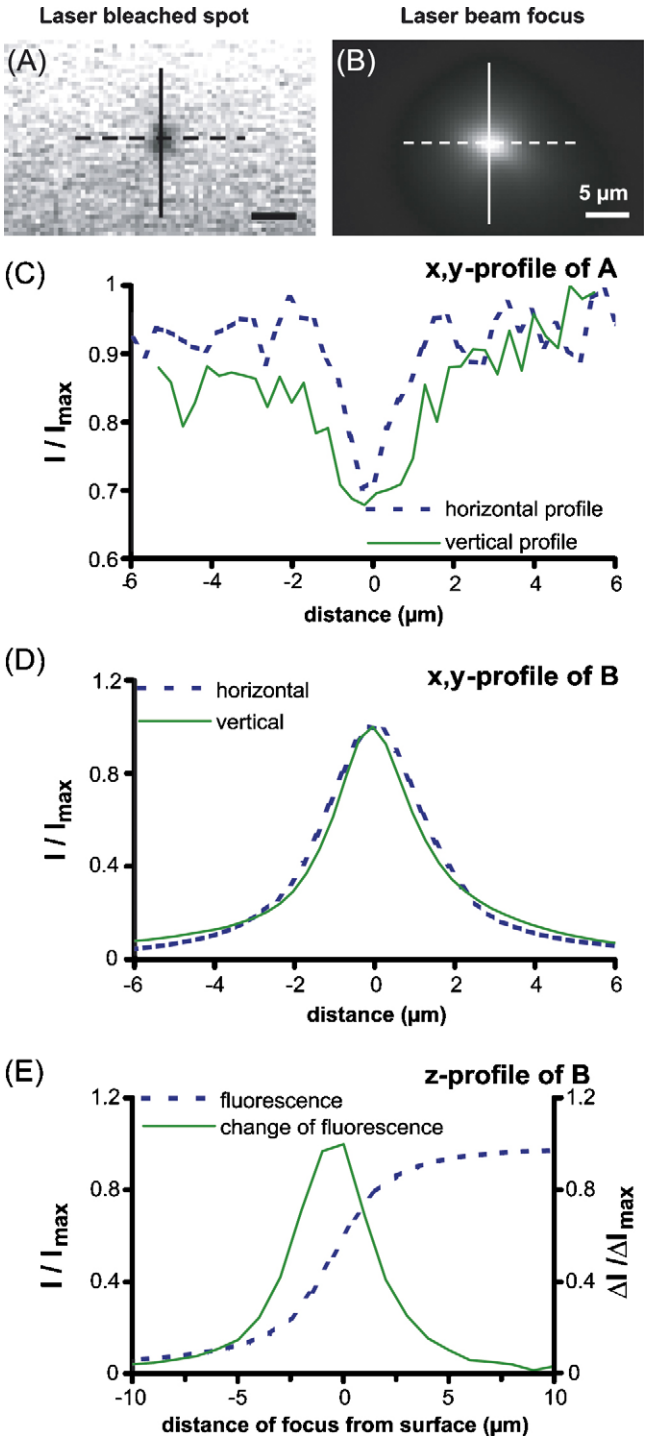

Fig. 5. Laser focus spot size. (A) Bleaching of an orange polymer (Chroma) slide, by the focused 532 nm laser using the same optics employed for photoactivation. Shown is an image averaged from five bleached spots subsequently assessed by two-photon imaging. The image has been used to determine the horizontal (dashed line) and vertical (continuous line) dimension of the focused laser spot, which are plotted in panel C. (B) Wide-field CCD epifluorescence image of the surface of a Texas Red dextran containing agarose slab, used to estimate the dimensions of the focused laser spot in 3D, as plotted in panels D and E. (C) Horizontal and vertical profile of bleached spot in the fluorescent polymer slide shown in panel A. (D) Horizontal and vertical profile of fluorescence by the focused laser on the surface of Texas Red dextran agarose shown in panel B. (E) Estimate of the laser spot size in the *Z*-direction by taking the derivative of the plot of fluorescence signal versus scanning depth within the Texas Red dextran agarose sample.

that when the laser was focused on a vessel scattered light into adjacent tissue was reduced by an even larger extent (Fig. 6C). Analysis of the relationship between vessel size and attenuation (of scattered light) indicated that as expected the effects were more pronounced in larger vessels (Fig. 6D). These data in combination with estimates of Z focal volume using the agarose slab argue against significant photoactivation occurring below the surface artery that was targeted.

4. Discussion

With this paper, we provide an outline for construction of a simple photoactivation hardware device applicable for creating targeted strokes within *in vivo* preparations (Schaffer et al., 2006; Zhang and Murphy, 2007). In our hands, the laser system could reliably block individual brain arterioles within minutes of illumination in the presence of Rose Bengal. In the absence of photosensitizer Rose Bengal, we did not observe any direct effects of 2 mW of 532 nm laser power focused onto the brain (Zhang and Murphy, 2007).

Although we have employed the laser only for the photothrombotic method so far, we anticipate that a similar design could be used for local photoactivation of fluorescent proteins, i.e. photoactivatable GFPs (Ando et al., 2004), photobleaching of any dye, or uncaging of compounds such as caged tetracyclines to induce protein expression (Cambridge et al., 2006) with laser light of appropriate wavelength. It is conceivable that this device could be added to other microscope brands (than Olympus) that have a filter slot within their epifluorescence excitation pathway. If a slot does not exist one could be cut. One question is whether the photoactivation laser could employ other paths of entry, such as the vertical path taken by the two-photon excitation laser light (Fig. 1C, part 14)? This would certainly work, although the use of the fluorescence emission path to the CCD camera detection system (Fig. 1C, part 16) would need to be modified. If the 532 nm laser were directed through the vertical port, or if the laser from a commercial confocal were used, one would need to add a dichroic mirror within the DPMC-WI trinocular microscope tube (Fig. 1C, part 15) that would pass green excitation light, but reflect red emitted light to the camera. The use of a laser from a confocal microscope would still probably require a wide-field CCD camera to confirm the clotting process. In our hands placement of the laser in the epifluorescence path (Fig. 1C, part 12) was the simplest option. Another elegant option employed by the Kleinfeld lab is to place the green laser within the two-photon excitation path and to periodically photoactivate and image the specimen by alternating between green laser photoactivation and monitoring of blood flow using fluorescent dextran imaging by two-photon microscopy (Schaffer et al., 2006; Zhang and Murphy, 2007). This approach may allow for better monitoring of blood flow than epifluorescence since two-photon microscopy will have better depth penetration. However, the improved depth penetration of two-photon microscopy may not be necessary given surface vessels are usually targeted since they give rise to deeper penetrating circulation (Nishimura et al., 2007). To employ the two-photon light path a movable dichroic mirror or a dichroic mirror that passes both green and

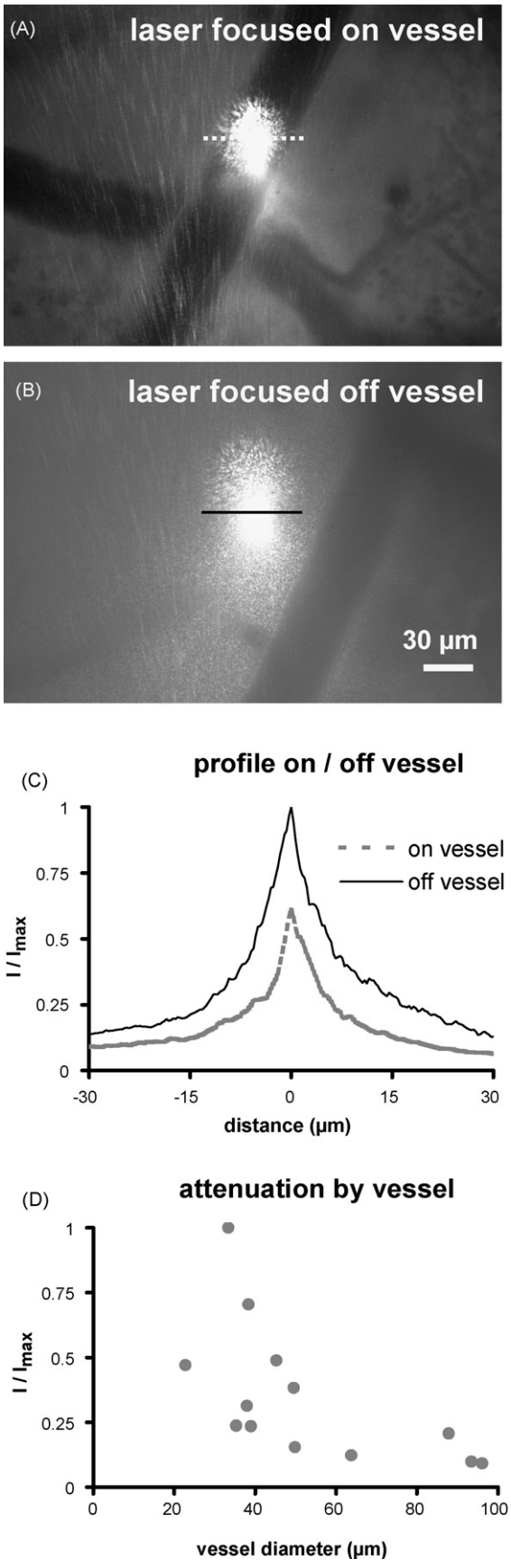

infrared light would be needed to alternate between two-photon and green laser excitation.

With regard to the dimensions of the photoactivation site using our laser system, we expect that these would be determined primarily by the extent to which the objective back aperture was filled and the numerical aperture of the objective used (Nolte et al., 2006; Stelzer, 2006). Typically, we have employed a 40×, 0.8 NA water immersion objective for *in vivo* photoactivation. Lateral resolution appears to be better than 3 μm from assessment of bleached fluorescent test slides and an agarose slab. Axial resolution was estimated to be better than 5 μm, suggesting that for most artery segments (>10 μm in diameter) the photoactivation process would be relatively selective. It is possible to increase excitation focal volume further to tailor photoactivation for larger vessels by reducing the laser spot size at the objective back aperture as would be expected for other forms of microscopy (Stelzer, 2006). Although the photoactivation spot could be made larger by underfilling the objective, the excitation process appeared to be self-limiting due to strong absorbance of green light by the targeted surface blood vessels (see Fig. 6D). In practice, the parameters we used worked best for photoactivation within vessels that were 10–60 μm in diameter.

A direct method to assess sub-surface unintentional photoactivation would be to perform histology (Nishimura et al., 2007) and determine whether clotted capillaries were present under a targeted arteriole of interest. Although such an analysis is an elegant way to assess the presence of clots, it does not distinguish between clots which are created by the Rose Bengal photoactivation process and those which flowed downstream from a targeted arteriole. Because of this concern, we have not performed this analysis. However, off-target indirect subsurface clotting should be minimal since other investigators found that sub-surface vessels that were close to a targeted arteriole could be fully flowing provided that we fed by a parallel vascular network (Nishimura et al., 2007). These finding suggested that not all vessels in the vicinity of photoactivation undergo clotting. In general, to reduce off-target photoactivation, we suggest that investigators shield a Rose Bengal injected specimen from white or green light, use minimal laser power, and only activate their laser when it is focused on a vessel of interest. If off-target clot-

Fig. 6. Blood vessels strongly absorb green laser light minimizing off-target clotting in brain tissue. (A) Reflected green laser light from a blood vessel (arteriole) with the laser beam focused on it. The dotted line indicates the position where the profile in panel C where taken. (B) Light reflection from tissue with the laser beam focused 40 μm from the blood vessel. The broader distribution of scattered light and the brighter background indicate that light scattering is stronger if no blood vessel is targeted by the laser due to apparent green light absorption by the blood. (C) Horizontal profiles of light reflection from tissue with the laser beam targeted on the vessel (as shown in panel A) and away from it (as shown in panel B). The profiles are averaged from five separate vessels. Peak light scattering was reduced by about 50% by the presence of a vessel. However, even larger reductions in light scattering were observed in the shoulder regions of the profile due to the vessels effectively narrowing the intensity profile. (D) Stronger green light attenuation by larger blood vessels (arterioles). Shown is the reflectance of the green laser light by blood vessels of different diameters.

ting is observed, the Rose Bengal concentration injected can be reduced (see Section 2.1).

In conclusion, this hardware modification will allow users of commercial upright microscopes to readily perform targeted photoactivation or bleaching with minimal modification of their existing equipment.

Acknowledgements

We would like to thank Pumin Wang for his technical support. This work was supported by operating grants to THM (MOP49586) from Canadian Institutes of Health Research (CIHR) and the Canadian Stroke Network (THM). The In vivo Imaging Centre is supported by research resource support grant from CIHR.

Appendix A. Supplementary data

Supplementary data associated with this article can be found, in the online version, at doi:10.1016/j.jneumeth.2007.12.015.

References

Ajudua S, Mello MJ. Shedding some light on laser pointer eye injuries. Pediatr Emerg Care 2007;23:669–72.

Ando R, Mizuno H, Miyawaki A. Regulated fast nucleocytoplasmic shuttling observed by reversible protein highlighting. Science 2004;306:1370–3.

Biskup C, Böhmer A, Pusch R, Kelbauskas L, Gorshokov A, Majoul I, et al. Visualization of SHP-1-target interaction. J Cell Sci 2004;117:5165–78.

Briers JD, Webster S. Laser speckle contrast analysis (LASCA): a nonscanning, full-field technique for monitoring capillary blood flow. J Biomed Opt 1996;1:174–9.

Cambridge SB, Geissler D, Keller S, Cürten B. A caged doxycycline analogue for photoactivated gene expression. Angew Chem Int Ed Engl 2006;45:2229–31.

Du H, Fuh RA, Li J, Corkan A, Lindsey JS. PhotochemCAD: a computer-aided design and research tool in photochemistry. Photochem Photobiol 1998;68:141–2.

Dunn AK, Bolay H, Moskowitz MA, Boas DA. Dynamic imaging of cerebral blood flow using laser speckle. J Cereb Blood Flow Metab 2001;21:195–201.

Frostig RD, Lieke EE, Ts'o DY, Grinvald A. Cortical functional architecture and local coupling between neuronal activity and the microcirculation revealed by *in vivo* high-resolution optical imaging of intrinsic signals. Proc Natl Acad Sci USA 1990;87:6082–6.

Kleinfeld D, Denk W. Two-photon imaging of neocortical microcirculation. In: Yuste R, Lanni F, Konnerth A, editors. Imaging Neurons: A Laboratory Manual, 23. Cold Spring Harbor, NY: Cold Spring Harbor Laboratory Press; 2000. p. 1–15.

Kleinfeld D, Denk W. Two-photon imaging of cortical microcirculation. In: Yuste R, Konnerth A, editors. Imaging in Neuroscience and Development: A Laboratory Manual. Cold Spring Harbor, NY: Cold Spring Harbor Laboratory Press; 2005. p. 701–5.

Kleinfeld D, Mitra PP, Helmchen F, Denk W. Fluctuations and stimulus-induced changes in blood flow observed in individual capillaries in layers 2 through 4 of rat neocortex. Proc Natl Acad Sci USA 1998;95:15741–6.

Kleinfeld D, Friedman B, Lyden PD, Shih AY. Targeted occlusion to surface and deep vessels in neocortex via linear and nonlinear optical absorption. In: Chen J, Xu Z, Xu XM, Zhang J, editors. Animal Models of Acute Neurological Injuries. Totowa: Humana Press; 2008.

Nishimura N, Schaffer CB, Friedman B, Lyden PD, Kleinfeld D. Penetrating arterioles are a bottleneck in the perfusion of neocortex. Proc Natl Acad Sci USA 2007;104:365–70.

Nolte A, Pawley JB, Höring L. Non-laser light sources for three-dimensional microscopy. In: Pawley JB, editor. Handbook of Biological Confocal Microscopy. New York, NY: Springer; 2006. p. 126–44.

Schaffer CB, Friedman B, Nishimura N, Schroeder LF, Tsai PS, Ebner FF, et al. Two-photon imaging of cortical surface microvessels reveals a robust redistribution in blood flow after vascular occlusion. PLoS Biol 2006;4:e22.

Stelzer E. The intermediate optical system of laser-scanning confocal microscopes. In: Pawley JB, editor. Handbook of Biological Confocal Microscopy. New York, NY: Springer; 2006. p. 207–20.

Watson BD, Dietrich WD, Busto R, Wachtel MS, Ginsberg MD. Induction of reproducible brain infarction by photochemically initiated thrombosis. Ann Neurol 1985;17:497–504.

Zhang S, Murphy TH. Imaging the impact of cortical microcirculation on synaptic structure and sensory-evoked hemodynamic responses *in vivo*. PLoS Biol 2007;5:e119.

Zhang S, Boyd J, Delaney K, Murphy TH. Rapid reversible changes in dendritic spine structure *in vivo* gated by the degree of ischemia. J Neurosci 2005;25:5333–8.